Transport in Porous Media (2023) 147:305–330
https://doi.org/10.1007/s11242-023-01909-5

A Systematic Study on the Influence of Grain Characteristics on Hydraulic and Mechanical Performance of MICP-Treated Porous Media

Charalampos Konstantinou[1,2] · **Yuze Wang**[3,4] · **Giovanna Biscontin**[1]

Received: 25 June 2022 / Accepted: 23 January 2023 / Published online: 13 February 2023

Abstract

The bio-cementation of sands (microbially induced carbonate precipitation) is an emerging technique that could broaden the horizons in the sectors of hydraulics, hydrology and geo-environmental engineering. It has been used extensively to increase the strength of sands and for controlled permeability reduction. This study focuses on the choice of base materials and presents an extensive program to generate materials with various combinations of properties and assess the effects of grain shape, size and spread of particle size distributions on permeability, unconfined compressive strength and porosity. Better strength enhancement and more controlled permeability reduction is achieved for bio-treated specimens with a moderate number of particle-to-particle contacts (D_{50} = 180–890 μm). Results showed that the grain size has the greatest impact on both strength and permeability with very small (D_{50} = 110 μm) or very large grains (D_{50} = 1810 μm) not being effective in terms of strength enhancement and permeability control. The higher the uniformity coefficient of the base material is (D_{60}/D_{10} from 1.4 to 5.6), the greater the effects on the mechanical properties are because of the narrower pore space and the higher number of contact points between particles. Materials with higher uniformity coefficients and larger grain sizes (i.e., D_{60}/D_{10} = 5.6, D_{50} = 2454 μm) provide more controlled strength enhancement and permeability reduction. The particle shape either angular, subrounded, or spherical does not affect much the resulting mechanical properties as long as the grain sizes fall within a region compatible to the bacterial size (D_{50} = 180 and 890 μm).

Article Highlights

- MICP was applied successfully using a wide range of base granular materials.
- The grain size has the greatest impact on strength and permeability in bio-treatment against grain shape and PSD.
- Wider particle size distribution and larger grain size leads to controlled alteration of strength and permeability.

Extended author information available on the last page of the article

Keywords MICP performance · Grain characteristics · Particle size distribution · Permeability · Porosity · Strength

1 Introduction

Many applications in the field of civil, geo-environmental, hydraulics and hydrological engineering take place in weakly cemented granular materials in which the underlying principle is the flow of fluid in porous media. Some examples include soil stabilisation, grouting, liquefaction and erosion control, solidification of heavy metals, groundwater decontamination, hydraulic barriers, oil and gas storage, but also CO_2 or H_2 storage, transportation of various fluids in ground, sand control in natural gas production, etc.

Soft sands or weakly cemented and poorly consolidated sandstones represent transitional materials between soils and rocks and share common characteristics with both. ISRM (1981) classified rocks according to their strength based on UCS and soft sandstones fall in the categories of 'very weak' and 'extremely weak sandstones'. The quantification of the engineering properties of these materials (pore volume and network, permeability, strength) which are essential to many geophysical problems, although studied extensively, remains a challenge and imposes further restrictions in understanding processes that take place in weakly cemented porous media (Liu et al. 2022; Rubol et al. 2018; Wang and Kulatilake 2008; Zhao et al. 2021). This is because coring of soft sandstones is a challenging procedure. Traditional sampling methods frequently degrade cementation, resulting in poor recoveries making it difficult and expensive to obtain enough high-quality samples for laboratory testing.

Artificial rock specimens, on the other hand, can provide almost endless quantities and a wide range of features, allowing for the independent control of the required structural properties and the isolation of the effects of those variations. The reconstitution of a certain geological material usually requires the characterization and laboratory replication of the geological processes that occurred in nature, even if the impossibility of reproducing the effects of geological time must be recognised. There exist two fundamental requirements for samples, the uniformity of behaviour and the degree of similarity with average natural behaviour.

This research presents a parametric study to create artificial specimens via microbially induced carbonate precipitation (MICP), a bio-cementation method used to increase the amount of cementation within a granular network, to be used as a proxy in more complex laboratory testing and for designing MICP field experiments related to the listed applications. The study isolates and examines influence of the granular media characteristics on hydraulic and mechanical performance of the MICP-treated porous media by keeping the characteristics (size and type) of the precipitating carbonate crystals fixed as the MICP parameters remain the same (the protocol remains fixed). The conjugate changes and combinations of strength, permeability and porosity are also evaluated for which little work has been conducted previously. Previous research on MICP-treated granular media cannot be combined as the choice of the MICP parameters significantly affects the type and size of the precipitating calcium carbonate crystals which in turn affects the resulting medium properties. The study also explores further the capabilities of the MICP method on base materials with various grain sizes, shapes, and widths of particle size distributions (PSDs) which have not been considered as good candidates for bio-cementation.

2 Background

Amongst its numerous applications in civil, geo-environmental and hydraulics engineering, microbially induced carbonate precipitation (MICP) has been proposed as a technique to generate artificial sandstones by cementing a granular matrix (Konstantinou et al. 2021a; Konstantinou and Biscontin 2021; Marzin et al. 2020) and to seal fractured rocks (Tobler et al. 2018; Weinhardt et al. 2021). Along the same direction, MICP can be used to study the transition from soil to rock and the effects of progressively increasing cohesion. The bio-treated specimens allow to examine independently the effects of cementation characteristics and amount, as well as the impact of the intrinsic properties of the constituents on the resulting material properties, such us permeability, porosity and strength. At the same time, the developed weakly cemented bio-treated media could be used as a substitute of natural sandstones in laboratory testing to study fluid flows in both soils and rocks which are of great interest in the research community (Alqahtani et al. 2022; Gao et al. 2020; Hussain et al. 2014; Konstantinou and Biscontin 2022; Lima et al. 2020; Saxena et al. 2019a, b; Scott et al. 2019; Torskaya et al. 2014; Wang et al. 2022a; Yu et al. 2018). Many studies have assessed the strength of MICP products; however very few studies consider porosity and permeability usually through modelling (Wang and Nackenhorst 2020).

It is widely recognised that the effectiveness of MICP depends on a successful recipe formulation which relies on the selection of a combination of bio-chemical parameters based on the required application. Such parameters include bacterial population and urease activity, chemical solution concentration, injecting method, retention time (duration between two subsequent injections), urea to calcium chloride ratio, etc. (Barkouki et al. 2011; Cheng et al. 2017; DeJong et al. 2010; Konstantinou et al. 2021c; Mortensen et al. 2011; Al Qabany et al. 2012; Wang et al. 2022b, 2021, 2019; van Wijngaarden et al. 2016).

In recent years, apart from the bio-chemical parameters, the material's intrinsic properties have been recognised as part of the design process of an effective formulation (Dadda et al. 2019; Terzis and Laloui 2019, 2018; Xiao et al. 2019). Although the importance of material's intrinsic characteristics is often highlighted, very few studies concerning the role of granular medium characteristic factors on the MICP engineering response exist. The effect of relative density of the base material has been extensively investigated in relation to the mechanical properties of the MICP-treated specimens (Al Qabany et al. 2012; Gao et al. 2019; van Paassen 2009) but only recently, factors like grain size, percentage of fines and grain shapes have been investigated (Mahawish et al. 2018a; Terzis and Laloui 2019, 2018; Xiao et al. 2019).

The engineering properties of the cemented specimens depend on the initial configuration of the base material (particle shape, size, spread of particle size distribution-PSD) and the morphology and distribution of the carbonate crystals relative to the grains (Burbank et al. 2013; Cheng et al. 2017; DeJong et al. 2010; Konstantinou et al. 2021b; Mujah et al. 2017; Al Qabany et al. 2012). The mechanical properties though, vary from study to study depending on the selection of the bio-chemical parameters and overall, on the experimental protocol which makes it difficult to combine the findings. The key to assessing the effects of each parameter (both biological or grain-related) is to isolate the rest of the effects and follow a consistent recipe.

While several procedures have been developed to optimise MICP using a single type of sand, limited research has been conducted to assess the effectiveness of the process for a wide range of particle sizes. The vast majority of previous research utilises uniform sands with average particle diameters of 0.15–0.7 mm (Cheng et al. 2017;

Cui et al. 2017; Feng and Montoya 2015; Al Qabany and Soga 2013). Only few studies are based on very fine or very coarse sand for bio-treatment (Konstantinou et al. 2021a; Mahawish et al. 2018b) mainly because of the difficulties experienced when small or large pores exist (D_{10} in the range between 80 and 110 um) (Mitchell and Santamarina 2005; Rebata-Landa 2007). Cheng et al. (2013) compared the strength gain for sands with D_{50} of 0.25 and 0.7 mm and concluded that fine sands exhibited significantly higher cohesion compared to coarse sands, while coarse sands had higher gains in friction angles. Terzis and Laloui (2018) used fine and medium grained sands (average grain size 0.19 and 0.39 mm, respectively) and showed a more pronounced improvement in stiffness of the medium-grained material because larger calcium carbonate crystals were formed. The use of base materials with a wider range of grain sizes would enable a broader variety of combinations of strength, permeability, and porosity.

The particle size is just one of the grain characteristics that could significantly affect the achievable engineering properties of the bio-treated specimens. The grain shape and spread of the particle size distribution (PSD) also affect the strength even without the addition of cementation. Angular particles can form more open, less dense structures compared to spherical grains providing a lower number of contact points between the particles compared thus a lower number of grain-to-grain contacts which are effective locations for cementation to occur (Ismail et al. 2002). However, Xiao et al. (2019) investigated the role of shape geometry on strength gain, demonstrating that the secant modulus E_{50} decreased with increasing roundness of the particles for a given cementation level. Further work needs to be carried out to assess the effects of shape geometry in relation to the grain size and the precipitating carbonate crystals.

A well graded sand is characterised by a small-sized pore network configuration and has more particle-to-particle contact points. The degree of sorting, i.e. the uniformity coefficient (D_{60}/D_{10}), is another important parameter that needs to be taken into account when assessing strength enhancement and permeability reduction. The relationship between width of particle size curves, the properties of the bio-treated specimens and the overall MICP engineering response needs to be assessed systematically as the literature lacks such studies.

This paper presents a comprehensive study of the effects of grain shape, size and width of PSDs on the resulting mechanical and physical properties, in particular permeability, unconfined compressive strength (UCS) and porosity, which are the basic properties of interest in groundwater investigations, by cementing twelve different base materials at various cementation levels. The study pushes the typical boundaries of the MICP method by cementing base materials that are not considered as optimum candidates for bio-treatment and therefore have not been used previously providing successfully uniformity in behaviour. A consistent recipe/formulation was followed across the testing program, only altering the amount of injected cementation solution to achieve the targeted cementation levels. The study presents a wide range of achievable combinations of UCS, permeability, porosity and pore network distribution in bio-cemented sands which could be used as a proxy for natural granular media (in shallow and intermediate depths) ensuring sufficient similarity with average natural behaviour. The findings are also applicable to designing MICP field applications. Based on the initial properties of the granular medium, a resulting strength, permeability, and porosity could be targeted prior to implementing the method in the field.

3 Methods

3.1 Granular Materials

Twelve types of sands were used to investigate the effects of grain size on the resulting properties of bio-cemented specimens via MICP: very fine sand, fine sand, medium grained sand, coarse sand, very coarse sand and gravel. The PSDs are shown in Fig. 1 and the grain characteristics and initial porosity are shown in Table 1. Sands 1–6 were utilised to study the effects of the grain size. All were uniform with very similar coefficients of uniformity (defined as the ratio of D_{60} to D_{10}) and had sub-rounded grains with medium sphericity, whilst gravel had a larger uniformity coefficient.

Three mixtures of sands (10–12) were used to vary the uniformity coefficient (D_{60}/D_{10}). A poorly graded soil has a uniformity coefficient of less than 4. Mixture 1 had a low uniformity coefficient ($C_u = 2.22$) while mixtures 2 and 3 had roughly the same uniformity coefficients (around 5).

The effects of the particle shapes on the engineering properties of the treated products were examined with three materials: fine and coarse glass beads, and Hostun sand. The glass beads had a spherical shape with average particle size of approximately 180 µm and 1770 µm, whilst Hostun sand was sub-angular, with average grain size 371 µm as shown in Fig. 1 and Table 1. The three types of grains were compared to subrounded sands with similar grain sizes. Fine glass beads were compared to fine sand, coarse glass beads to coarse sand and Hostun sand to medium-grained sand.

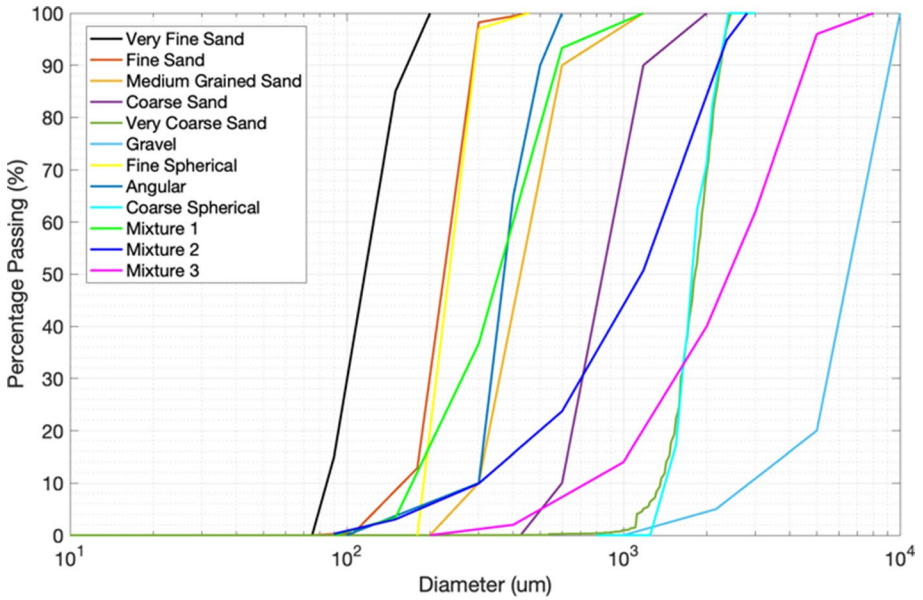

Fig. 1 PSD curves for the granular material used in this study

Table 1 The various base materials used in this study and their characteristics (average particle diameter, grain shape, uniformity coefficient and initial porosity)

	Type of sand	Average particle diameter	Particle shape	Uniformity coefficient (Cu)	Initial porosity ($\mu \pm \sigma$)
1	Very fine-Fraction E	110 μm	Sub-rounded	1.51	0.431 ± 0.023
2	Fine-Fraction D	180 μm	Sub-rounded	1.38	0.423 ± 0.009
3	Medium grained-Fraction C	450 μm	Sub-rounded	1.63	0.406 ± 0.006
4	Coarse –Fraction B	890 μm	Sub-rounded	1.60	0.384 ± 0.009
5	Very coarse-Fraction A	1810 μm	Sub-rounded	1.33	0.375 ± 0.021
6	Gravel	6100 μm	–	2.33	0.367 ± 0.024
7	Fine Glass beads	240 μm	Spherical	1.32	0.414 ± 0.019
8	Hostun sand	372 μm	Sub-angular	1.30	0.464 ± 0.009
9	Coarse Glass beads	1772 μm	Spherical	1.29	0.349 ± 0.008
10	Mixture 1	371 μm	Sub-rounded	2.22	0.345 ± 0.008
11	Mixture 2	1180 μm	Sub-rounded	5.60	0.331 ± 0.015
12	Mixture 3	2454 μm	Sub-rounded	4.62	0.335 ± 0.024

3.2 Generation of Artificial Specimens

The MICP formulation is described in detail in Konstantinou et al. (2021a, b, c) and summarised here. The sand was placed in cylindrical molds of 35.4 mm in diameter and 110 mm in height and vibrated to reach a targeted porosity. The final height of the specimens was 71 mm. The injection direction of the bacterial suspension and cementation solution was from top to bottom via gravity (see a schematic of the experimental setup in Fig. 2). The bacterial solution (*Sporosarcina pasteurii*, OD600 between 1.5 and 2.0, average urease activity of 0.8 mM urea/h/OD) was only injected once at the beginning of the

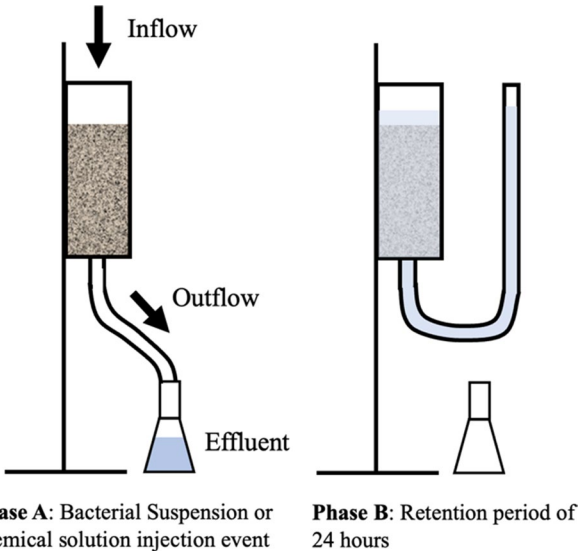

Fig. 2 Experimental setup—stepwise injection via gravity: Phase A—injection; and Phase B—retention period

process. Before each new chemical solution injection (0.375 M urea, 0.25 M calcium chloride, 3 g/L nutrient broth), the excess solution was allowed to freely drain out and then the new chemical solution was introduced (phase A—injection event in Fig. 2). The time between two subsequent injections was 24 h for both bacteria and cementation injections (phase B—retention period in Fig. 2). In both phases (injection and retention period), the granular samples remained saturated. The level of cementation was controlled by the number of cementation solution injections. Higher number of cementation solution injections resulted in higher amount of carbonate in the final product. After the end of the last retention period specimens were extracted from the molds with care to minimise disturbance.

3.3 Carbonate Content

Carbonate content was measured according to the procedure in ASTM (2014). A 30 g dried and ground sample was treated with 30 mL of hydrochloric acid (HCl) in a chamber (calcimeter). The pressure reading from as resealed into the chamber by the reaction was correlated to the amount of calcium carbonate in the specimen. In this study, the degree of cementation is expressed as weight of calcium carbonate over the total weight of the sample tested (in percent).

3.4 Permeability Tests

Falling head tests using the injection molds as rigid wall permeameters were carried out to measure the permeability of specimens once the injection process was complete and before they were demolded. Permeability was measured after flushing 3 pore volumes of de-ionised water and assessed multiple times until the last three measurements agreed. When the permeability of the soil becomes small, rigid walls may not be suitable as the flow at the boundary between the wall and the specimen may be bigger than the flow through the actual specimen (Al Qabany et al. 2013). For this reason, the specimens' permeability was measured before removing the sample from the mould in order to minimise the boundary-specimen effects.

3.5 Unconfined Compressive Strength

Unconfined compressive strength (UCS) tests were performed on oven-dried specimens (105 °C for 24 h) with varying levels of cementation. The specimens were tested according to ASTM (2004) with displacement-controlled loading at a rate of 1.14 mm/min.

3.6 Final Porosity

The final porosity (n), defined as $n = 1 - \frac{\rho}{G_s}$ was calculated with bulk density (ρ) an equivalent specific gravity (G_s) that takes into account the specific gravities of the individual minerals present based on the relative volume fraction (Sharwood 1912):

$$G_s = \frac{W_{\text{total}}}{\frac{w_1}{G_{s1}} + \frac{w_2}{G_{s2}}}$$

where W_{total} is the total dry weight of the artificial material, w_1 and w_2 are the weight of quartz and carbonate, respectively. G_{s1} and G_{s2} are the specific gravities the of quartz and calcium carbonate, equal to 2.65 and 2.71 respectively.

3.7 MicroCT Imaging

Moderately cemented specimens across all base materials were imaged with the X-ray μ-CT high energy micro-tomography scanner (X-Tec Systems) with the following settings: 160 kV, 110 uA with a use of a 0.5 mm copper filter. The voxel sizes of the images were around 25–30 μm. Figure 3 presents a schematic of the process followed to calculate porosity and pore space distribution. Stacks of images were obtained and transferred to the ImageJ software (Rueden et al. 2017; Schindelin et al. 2012). Windows of 20*20 mm were extracted from the stack which were binarised and analysed via the BoneJ plugin to obtain the porosity and distribution of voids (Doube et al. 2010; Dougherty and Kunzelmann 2007). The segmentation (binarisation) of each slice was conducted with the IsoData algorithm (i.e., the iterative intermeans method). By setting an initial threshold and then computing the averages of the pixels above and below the threshold, the technique separates the image into object and background. The threshold is increased, the averages of those two values are calculated, and the process is repeated until the threshold exceeds the composite average. A cubic specimen (20*20*20 mm) was constructed with the binarised stack.

The porosity was calculated based on the volume fraction function of BoneJ for cuboids of 2 mm thickness across a 20 mm height of each sample. The pore space size histograms were calculated for the cuboid at the middle of the cube (10–12 mm thickness) utilising the

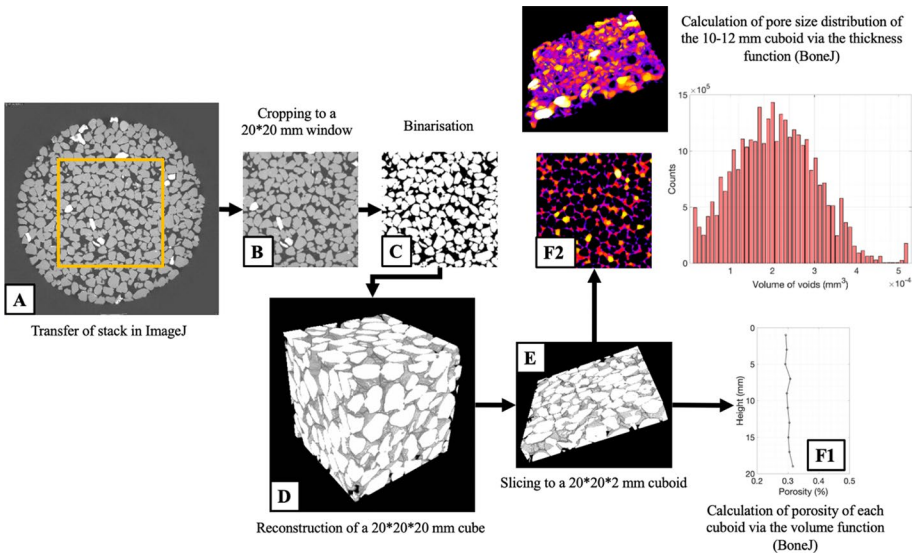

Fig. 3 The calculation of porosity and pore space distribution based on the MicroCT images: **a** the image stack was transferred to ImageJ, **b** a 20-by-20 mm window was extracted in each slice, **c** the images were binarised, **d** a cubic specimen with 2020*20 mm was reconstructed which **e** was sliced to a 20*20*2 mm cuboid. (F1) The porosity was calculated via the 'volume' function of BoneJ and (F2) the pore space was calculated via the 'thickness' function of BoneJ for the 10–12 mm cuboid

local thickness at a point, defined as the diameter of the largest sphere that fits within the available structure whilst also containing the point.

4 Results

This paper examines the effects of the grain size and shape, and spread of particle size distribution on permeability, strength, and porosity of the bio-cemented specimens. Grain size, spread of particle size distribution and grain shape on permeability, strength and porosity are examined separately in each sub-section. The uniformity of porosity is examined across the height of the specimens while the pore size distribution is evaluated for all twelve materials.

4.1 Grain Size

Sub-rounded sands with similar uniformity coefficients but different mean particle size (sands 1–6) were compared to examine the effect of grain size on strength gain, permeability and porosity reduction at various cementation levels (Fig. 4). A similar trend in reduction of permeability with respect to cementation level was observed for very fine sand through coarse-grained sand, with a progressively larger reduction as grain size increased. Very coarse sand and gravel did not follow the same trend, presenting permeabilities lower than medium- and coarse-grained sand in the range of cementation

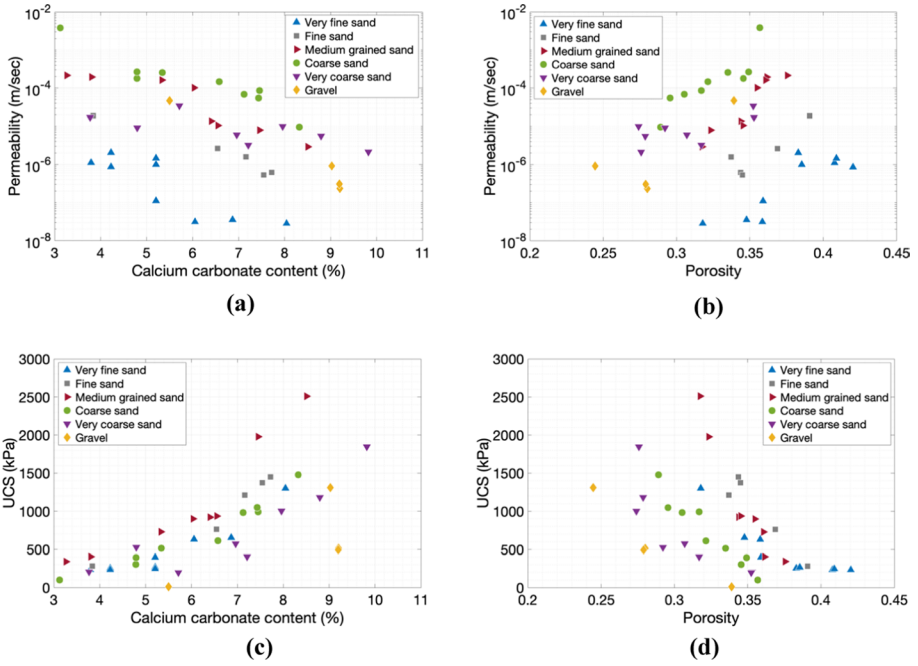

Fig. 4 Permeability with respect to: **a** calcium carbonate content (%), **b** porosity; UCS with respect to: **c** calcium carbonate content (%), **d** porosity

levels examined in the study. However, the reduction as the cementation level increased was less pronounced compared to the rest of the sands. Gravel's permeability seemed to experience the highest decline compared to the uncemented gravel, falling to around 6×10^{-6} m/sec when the cementation level was around 9%, which was lower than the permeability of coarse sands and almost equal to the permeability of fine sands.

As shown in Fig. 4c, the sands had similar strength of 200 kPa at around 3% cementation level but, as the cementation level increased, strength deviated substantially. Medium grained sands showed the highest strength across all cementation levels with an estimated UCS value at 10% calcium carbonate content reaching approximately 3500–3700 kPa, followed by fine and coarse sands with average particle diameter of 180 um and 890 um, respectively. Very fine sands had a strength of about 2800 kPa at the high cementation level, while very coarse sands had an estimated UCS value of about 1800 kPa.

Cemented gravel did not gain sufficient overall cohesion to carry out an unconfined compressive strength test until a large level of cementation of around 9% (Fig. 4c). Even then, the results are scattered. At 9% cementation the strength varied from 500 kPa to almost 1500 kPa. Generally, gravel presents very large pores, even if its porosity was very low as seen in Fig. 4b, d. Without any cementation, the porosity was found to be around 0.34 whilst for 9% cementation it decreased to about 0.23. Porosity and cementation level cannot describe solely the variations in permeability and strength with respect to gravel as the grains were too large and the pore network configuration largely depends on packing and how the grains are arranged next to each other. This is illustrated in Fig. 5b, where the porosity profile of gravel across the height the specimen of about 20 mm is shown to vary significantly.

The results can also be examined in relation to porosity of the cemented material. The increase in cementation relates directly to decreased porosity and therefore lower permeability (Fig. 4c) and higher strength (Fig. 4d). Very coarse and coarse sands porosities varied within the range between 0.28 and 0.35 while medium grained, fine and very fine sands had a porosity falling in the range between 0.32 and 0.42. The trends in hydraulic conductivities across sands 1–4 were similar with respect to porosities (Fig. 4d) while the sands with larger grains showed less dependence of permeability with respect to porosity.

At high porosity, fine and very fine sands had almost the same strength, but fine sands gain was larger at lower porosity (Fig. 4d). The trend of strength vs porosity for the other sands and gravel was similar, although shifted towards lower porosity levels.

Greater improvement in mechanical and hydraulic properties occurs in the medium-grained sand with an average particle size diameter of 450 um. The fine sands and coarse sands follow with slightly lower strengths. The strengths across the various cementation levels for finer and coarser sands are of similar magnitude allowing for various combinations of porosities and permeabilities to be achieved for a targeted strength level in lab experiments where flow in porous media is to be studied.

MicroCT images of moderately cemented specimens were taken to assess pore size and cementation deposits (Fig. 5). The pore network depends on the configuration of the particles within the porous matrix (initial porosity and grain size) and on the cementation characteristics (amount of cementation, crystal size and position). The porosity was generally uniform across the height of the specimens where sand was the base material and this was because of the relatively uniform deposition of the carbonate crystals. This particular combination of MICP parameters was implemented as it provided a balance of slower MICP reactions, through low urease activity and low concentration of the cementation solution, compared to the rate of flow with gravity injections, allowing uniform distribution

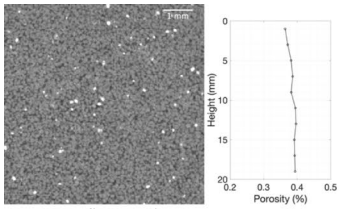

Very fine sand

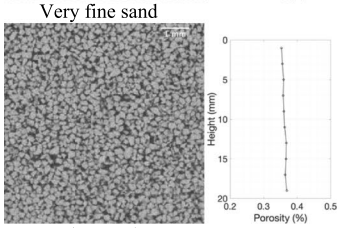

Fine sand

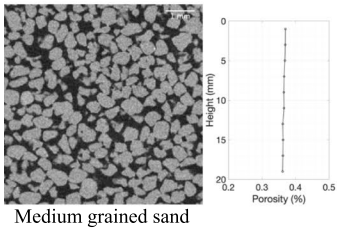

Medium grained sand

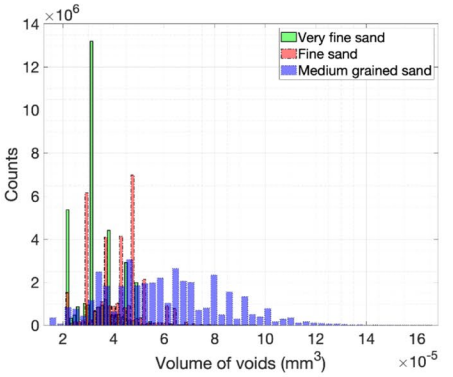

(a)

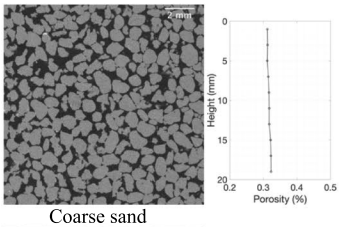

Coarse sand

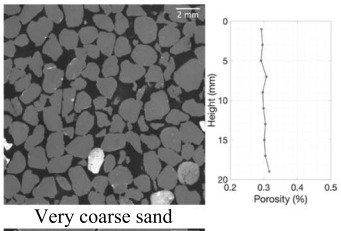

Very coarse sand

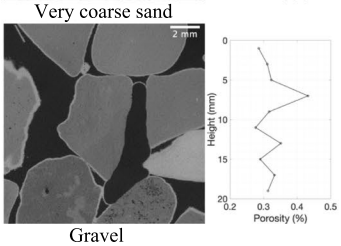

Gravel

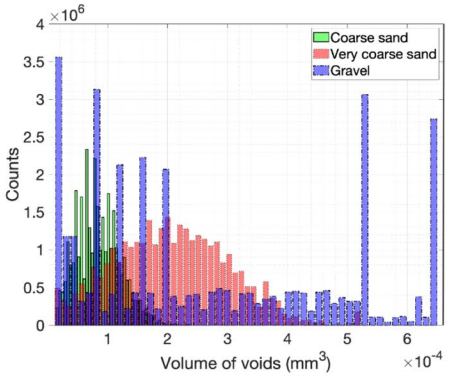

(b)

Fig. 5 Porosity distribution across the height of the samples and histograms demonstrating the pore size distribution (**a**) for very fine, fine and, medium grained sands (**b**) for coarse, very coarse sands and gravel

of bacteria and chemicals without clogging. The long retention times promoted efficient formation of carbonate.

Gravel's porosity showed substantial deviation and randomness due to the very large grains. The range of void sizes in very fine sand is very narrow (2—4×10^{-5} mm^3) and it spreads out as the grain size increases, while the peak value (frequency) decreases. The range pore sizes for fine, medium grained and coarse sands is wider (between 4×10^{-5} and 1×10^{-4} mm^3), while very coarse sand and gravel present a range between 2 and 7×10^{-5} mm^3.

4.2 Spread of PSD

The effect of the spread of the PSD was examined with three mixtures of poorly sorted sands. All grains had sub-rounded shape. Mixtures 1 and 2 had similar D_{10} which is a characteristic value used to define the uniformity coefficient. Mixture 3 had a similar shape of the PSD curve to Mixture 2's, however, shifted by about 1000 μm. Figure 6 compares the results for fine sands with average particle diameter of 180 μm and uniformity coefficient of 1.38, Mixture 1 ($D_{50}=371$ μm, Cu = 2.22), Mixture 2 ($D_{50}=1180$ μm, Cu = 5.6), and Mixture 3 ($D_{50}=2454$ μm, Cu = 4.62) at various cementation levels.

Mixture 1, which had a smaller average grain size, showed the lowest permeability values of all cementation levels falling in the range between 10^{-6} and 10^{-8} m/s (Fig. 6a). The rate of reduction with calcium carbonate content, though, was smaller than that of poorly graded fine sands. The particle sizes of the two materials were similar, however, a

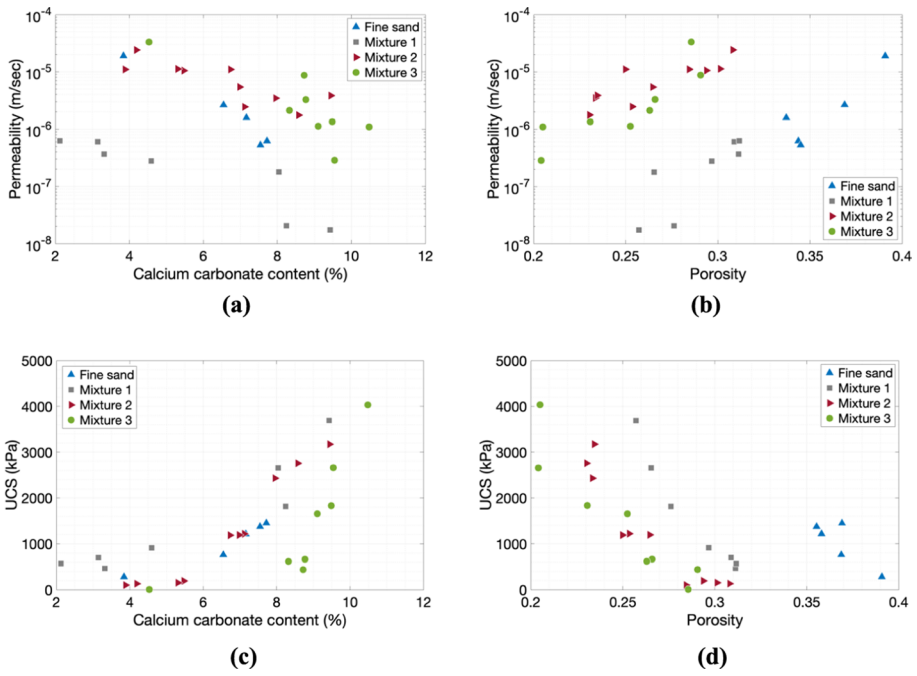

Fig. 6 Permeability with respect to: **a** calcium carbonate content (%), **b** porosity; UCS with respect to: **c** calcium carbonate content (%), **d** porosity

small increase in uniformity coefficient allows more efficient packing, lower porosity and, therefore, a reduction of permeability, even before cementation (Fig. 6b). Mixtures 2 and 3 had higher permeability compared to both fine sand and Mixture 1 because of their significantly larger content of particles, which also resulted in smaller porosities between 0.25 and 0.33 (Fig. 6b). However, they had lower permeability compared to coarse sands and gravel because of the much higher uniformity coefficient and more effective packing. The trend of permeability of Mixtures 2 and 3 with respect to the cementation level follows the behaviour of coarse sands. Mixture 3, which had almost the same uniformity coefficient as Mixture 2, but much larger particle sizes, essentially shows the same range of permeability as Mixture 2, indicating that the uniformity coefficient is more dominant than the grain size. The two mixtures overlap in their common region of porosities as shown in Fig. 6b.

The strength enhancement was more pronounced in Mixture 1 compared to specimens with fine sand as the base material (Fig. 6c). The average grain was of similar size, so the difference can be attributed to the variations in the uniformity coefficient. The trend in strength with respect to cementation level was similar to that of fine sands at low carbonate content, however, it deviated above 8% cementation. Mixture 1 was cemented more effectively at low cementation levels and specimens showed measurable strength even at 2% cementation. Fine sand at 4% cementation was still relatively unstable, with low strength (200 kPa).

Mixtures 2 and 3 need progressively higher cementation than Mixture 1 to achieve measurable strength (Fig. 6c). However, the rate of strength increase was more pronounced. The results showed that UCS values with respect to degree of cementation were similar but for mixture 3 shifted by about 2%, in the right, to achieve the same strength (up to 4000 kPa). The effects of the spread of the PSD on UCS and porosity of the bio-cemented materials are shown in Fig. 6d, where even a small increase of the uniformity coefficient results in a significant reduction of porosity (fine sands have a porosity of 0.35–0.4, Mixtures 1,2 and 3 have a porosity in the range between 0.2 and 0.33).

The distribution of porosity across the height of the specimens of the three mixtures was less uniform (Fig. 7) compared to the fine to coarse sands (Fig. 5). Mixture 1 shows a marginal trend of increasing porosity across the height of the specimen. Its pore network was very narrow with volumes of voids between 2 and 5×10^{-5} mm^3 and the observed gradient might be related to the flow reduction during treatment due to the initially lower porosity of the uncemented material. The distribution of pores was wider with smaller peaks and the pore volume was larger in Mixtures 2 ($0.3–2 \times 10^{-4}$ mm^3) and 3 ($0.5–4 \times 10^{-4}$ mm^3), since the grain sizes and the uniformity coefficients were larger. Mixtures 2 and 3, have narrower pore size distributions compared to the very coarse uniform sands because of the higher uniformity coefficient.

4.3 Grain Shape

Three pairs of base materials were used for this investigation. The first pair included fine sands of sub-rounded shape and fine glass beads with average particle size of about 240 um and uniformity coefficient of 1.32–1.33. The second pair included coarse sands of sub-rounded shape and coarse glass beads with average particle size of about 1180 um and uniformity coefficient of 1.29–1.33. The third pair examined two sands of similar average particle sizes (371–450 um) and of similar uniformity coefficients, but one had sub-rounded particles and the other angular.

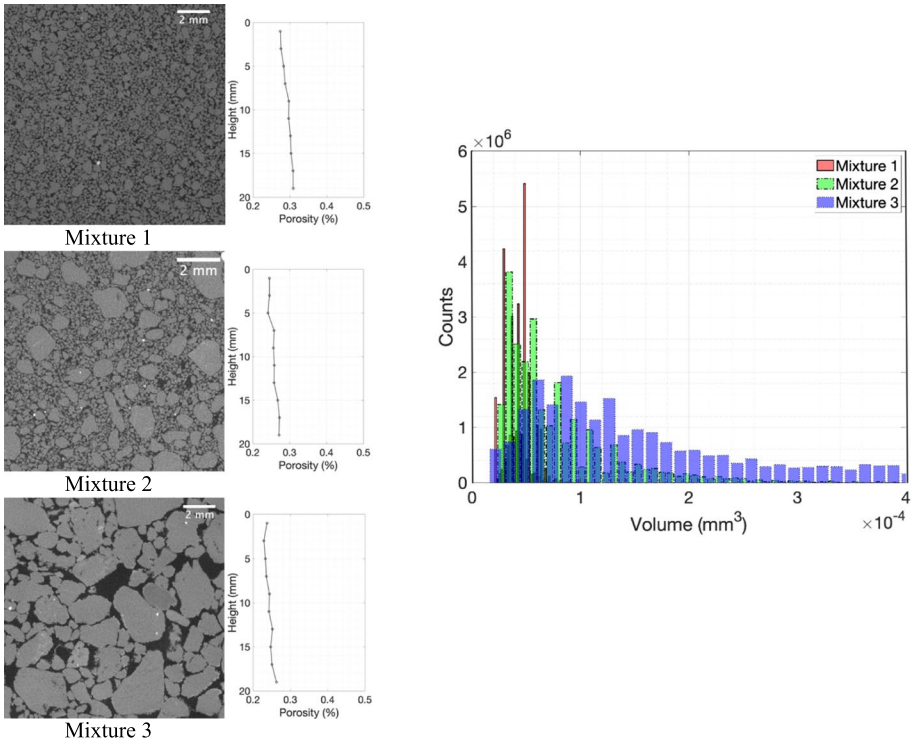

Fig. 7 Porosity distribution across the height of the samples and histograms demonstrating the pore size distribution for the three mixtures of sand

The main difference between base materials with different particle shape relates to packing density. Angular particles are more likely to have more contacts than spheres, especially monodispersed spheres. On the other hand, spheres tend to make very dense packings because of this. Angular particles can form more open, less dense structures. Vibration densifies them, but the assemblies are still more likely to have a higher porosity than spheres because of the role of asperities in enabling more open structures. Figure 8a shows the permeabilities of glass beads and sub-rounded sands at two particle sizes (the first two pairs). The fine spheres did not show any deviation from the fine subrounded sands in terms of permeabilities, as they showed a very similar trend with values between 10^{-5} and 10^{-7} m/sec. The same behaviour was observed at larger grain sizes (similar trend and range of permeability between (10^{-6} and 10^{-4} m/sec) indicating that the behaviour was controlled by the pore sizes rather than the particle shapes. The permeability of fine sands and glass beads are similar with respect to porosity also overlapping in the range between 0.33 and 0.37 (Fig. 8b). The permeability of coarse sands shows a different rate of increase with respect to porosity compared to glass beads, which were more scattered giving a larger range of final porosities.

Although they had the same reduction in permeability as fine sands, cemented glass beads showed lower strength compared to sub-rounded sands within the whole range of tested cementation levels (see Fig. 8c). The results are similar when comparing grain shapes at larger grain sizes. The precipitation patterns in both materials, coarse glass beads

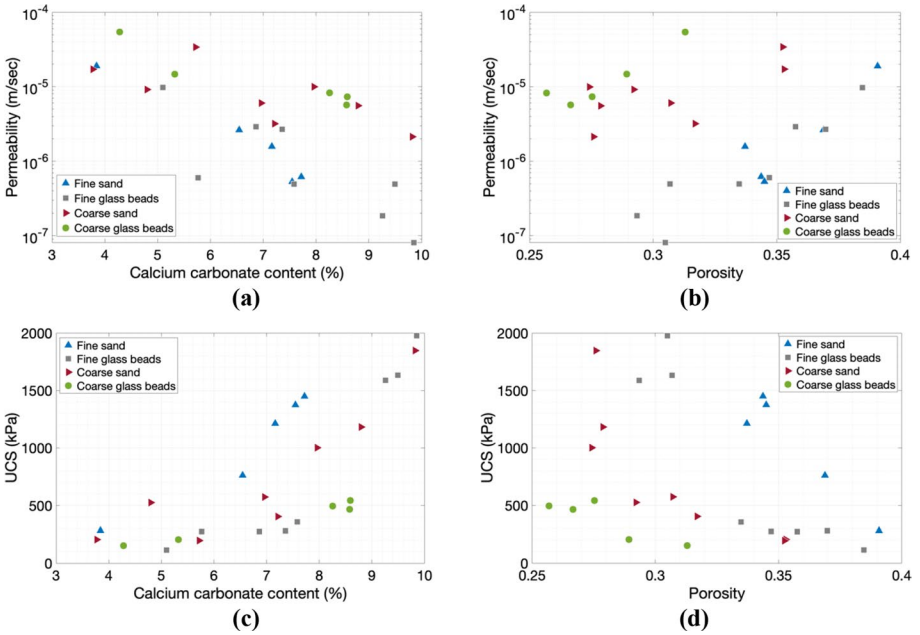

Fig. 8 UCS with respect to: **a** calcium carbonate content (%), **b** porosity for fine glass beads and UCS with respect to: **a** calcium carbonate content (%), **b** porosity for coarse glass beads

and very coarse sands, were very similar despite the differences that would be expected on surface bonding of carbonate on glass beads and on quartz; some crystals nucleated and grew on the surface of the particles and some on the contacts between the particles (Konstantinou et al. 2021a, b, c). Glass beads had lower UCS than corresponding rounded sands within the range of cementation levels investigated in this study. This is because glass was smoother and particles were round, so the failure tended to accrue at the glass-cement interface. The UCS of coarse glass beads over UCS of coarse sand ratio is similar to the UCS of fine glass beads to UCS of fine sand ratio at any carbonate content.

The UCS with respect to porosity results (Fig. 8d) were once again similar for both groups of grain sizes, however, as expected for the coarse particles the porosities were lower. The glass beads' porosity was also slightly lower compared to subrounded grains of the same grain size because of the denser packing that can be achieved. In addition, there is likely a difference in surface roughness as sand would be expected to have a higher particle-to-particle friction. The pore sizes of the glass beads, fine or coarse, were smaller compared to the subrounded sands are shown in the histograms of the pore size distributions shown in Fig. 9a, b. The two types of granular materials, glass beads and subrounded sands, had the same pore size distribution shape, while the porosity was more uniform across the height of the specimens for glass beads.

The third pair included a sub-angular grain base material contrasted to medium-grained sands with almost identical average particle sizes and uniformity coefficients. The reduction in permeability was similar across the sub-angular and sub-rounded sands (Fig. 10a), although the angular sand had higher permeability. The final product derived from cementation of angular sands had much higher porosity, in the range between 0.38 and 0.42, while the subrounded grained sands had a range between 0.32 and 0.38 (Fig. 10b). The slope in the plots of

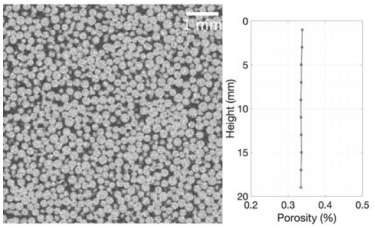

Fine glass beads

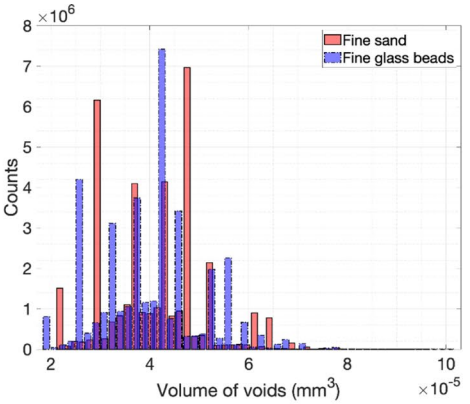

(a)

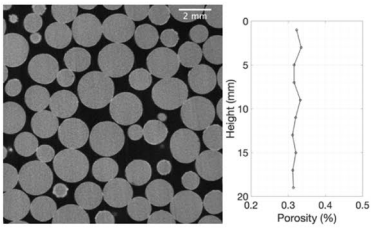

Coarse glass beads

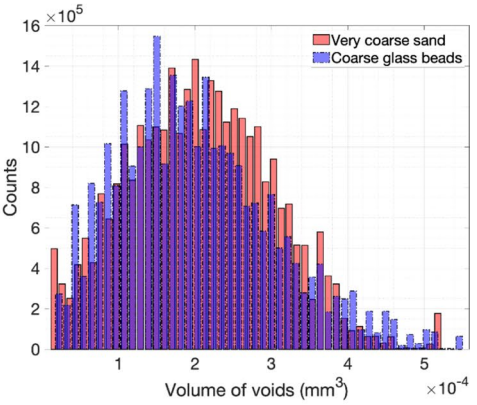

(b)

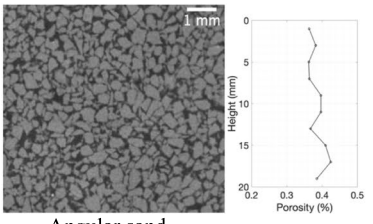

Angular sand

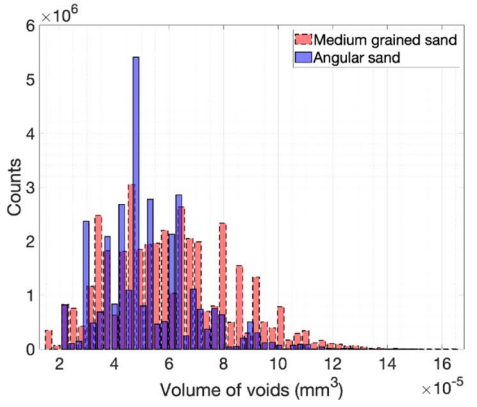

(c)

Fig. 9 Porosity distribution across the height of the samples and histograms demonstrating the pore size distribution **a** for fine glass beads, **b** for coarse glass beads, **c** for angular sand

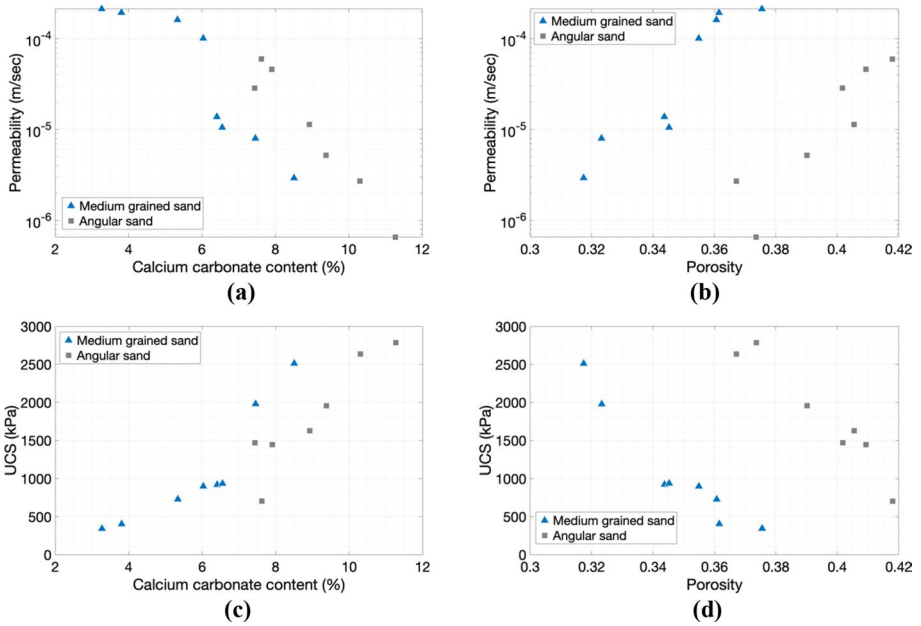

Fig. 10 UCS with respect to: **a** calcium carbonate content (%), **b** porosity for fine glass beads and UCS with respect to: **a** calcium carbonate content (%), **b** porosity for coarse glass beads

permeability with respect to porosity are the same for the two materials tested. The porosity profile of angular sands across the height of the specimens, provided higher variations as seen in Fig. 9c, while the pore size network distributions deviated substantially from the behaviour seen in most of the cases investigated. The subrounded sands reached higher strengths compared to the angular sands mostly because of the effect of shape on fabric (Fig. 10c). Angular particles stabilise in very open arrangements and can achieve stable fabrics at higher porosity than subrounded sands and glass beads.

5 Discussion

The base material significantly affects the mechanical and physical properties of the generated bio-cemented specimens. This study focuses on three of the most important properties which are widely used in the fields of hydrology, groundwater investigations and geotechnical engineering, namely, permeability, porosity, and strength. The effects of the grain size, spread of PSD and grain shape on permeability, porosity and strength are discussed in the current section. All three parameters are also affected by the carbonate precipitation patterns. The conjugate changes and combinations of the three properties are assessed and compared with the values presented for weakly cemented sands found in the literature as these materials could serve as a proxy for natural granular media.

5.1 Porosity and Pore Space

As the grain size increases the distribution of the pores becomes wider presenting smaller peaks (frequency of pore volume). Gravel showed porosity that varies significantly across the height of the specimen which is due to the very large grains that generate a pore network which is highly uneven. This is also reflected in the pore size distribution since gravel showed the wider distribution across all granular materials.

The pore network is significantly affected by the spread of the PSD. Even a small increase in the uniformity coefficient causes a high reduction in porosity. The pore size distribution is narrower with higher peaks as the uniformity coefficient increases. For example, Mixture 3 with higher D_{50} than the one of very coarse sand showed a narrower pore size distribution. This affects the flow of bacteria and chemical solutions during MICP treatment and hence the precipitation patterns which then influence the resulting properties.

The porosity is smaller in glass beads because of the denser packing, shifting the pore size distribution to the left where smaller pore volumes exist while the angular sand provided much higher variations in porosity. This irregularity is reflected in the pore distribution diagram (Fig. 9).

5.2 Strength

The strength of cemented materials depends on the number of contact points and on the location of the cementation. The higher the number of particles in a set volume (hence number of contact points) is, the higher the distribution of the stresses is within the granular matrix and thus, each particle experiences lower stresses. When cement is located at these contact points, it acts like glue, bonding the particles together. The strength of the bonds depends on the amount of cementation located around those contact points (effective cementation). In such case, the uncemented contact points become the weaker points between the particles. When particles are very large, higher probability exists of carbonate crystals nucleating on the surface of the particles providing less effective cementation. Thus, it is likely that a large portion of the precipitated cementation will land on less effective locations contributing less to strength enhancement. Whilst more contact points would provide more effective locations for cementation, too many contact points require larger overall amount of cementation in order to enhance strength because any un-cemented contact points create a preferential path of failure once compression is applied. Also, cementation can become random since flow during treatment is diverted from more densely packed areas to areas with less cementation.

The very coarse sands with an average particle diameter of 1820 μm had a lower number of particles, but more surface grain area providing more ineffective candidate spots for cementation. Therefore, the strength was consistently lower at any given cementation level. The very fine sands provided more contact points between the particles, offering more effective cementation locations, however, they had lower strength compared to fine sands. If there are many contact points to be cemented, then there will be inevitably some left without cementation support, hence, they would form weak points for a failure to occur, unless very high cementation is provided (above 10%). The fine to coarse sands provided the highest strength due to the balance between the absolute number of contact points and the ratio of contact points over surface grain area.

An increase in the uniformity coefficient results in the generation of more contact points and in the reduction of pore sizes, which in turn results in lower fluid flow through the porous medium during the MICP treatment procedure. Therefore, mixtures with larger particles and a wide PSD obtained better strength enhancement (large particles provide fewer contact points but this is compensated by the wider PSD which reduces the chances of cementation depositing on the particle surfaces). In materials with similar uniformity coefficients, but different grain sizes, larger cementation levels were required to achieve the same strength. This is because of the larger probability of cementation depositing on contact points between particles and not at the surfaces as the grains were smaller in size.

Particle shapes have very specific effects on the resulting mechanical properties. The grain shape that provided the higher strength is sub-rounded with spherical particles having too many contact points and angular particles not enough contact points. The angular particles have already an initial strength before any application of cementation due to interlocking. Cement provides an increase in strength, but interlocking is more effective (i.e., limited strength gain with cement increase).

5.3 Permeability

Permeability decreases significantly when the cement is found on the contact points and reduces the size of pore throats. For a material with higher number of particle-to-particle contacts, it is harder to reduce permeability since there are many contacts to be cemented. Such materials provide self-regulation of flow through paths with larger pores and pore throats which are likely to un-cemented particle contacts.

As the grain size of a packed bed of solids increases, the permeability is expected to increase also. For example, the Kozeny–Carman equation includes a squared average particle diameter in the nominator of the empirical equation. The same trend was observed for the cemented very fine to coarse sands of this study. The trend in reduction of permeability when more and more cementation was added to the base material was similar across these sands.

Very coarse sands and gravel did not follow the same trend showing a less controlled reduction. The precipitation of carbonate in very coarse materials is mainly on the surface of the particles rather than the contacts among the particles (Konstantinou 2021; Konstantinou et al. 2021a, b, c). The permeability then would not be expected to be reduced significantly. Despite this, the significantly lower number of contact points results in fewer options of flow paths which explains the rapid reduction of permeability in very coarse particles at lower cementation levels.

Gravel, which can only be compared to very coarse sand (both are considered ineffective for MICP treatment) shows larger reduction in permeability compared to very coarse sand, mainly because of the lower number of available flow paths. Gravel has an erratic pore distribution and randomness due to the very large grains providing very random paths for fluid flow. This is equivalent to having small pipes for flow and a few large pipes dominating the flow.

The permeability with respect to the cementation is lower when the base material has wider spread of PSD, because of the narrower initial pore space distribution before application of cementation. The trend in permeability reduction with respect to carbonate content is lower compared to more uniform sands because there are too many narrow flow paths to be cemented (and essentially close) when a higher number of contact points exists. This is the case for a granular material with a wide PSD. The absolute value and reduction of

permeability of two materials with similar uniformity coefficients but different grain sizes is the same, showing that the dominant factor that controls the flow is the spread of the PSD. Although the material with the smaller grain sizes had more contact points, it provided more flow path options compared to the one with larger grain sizes. At the same time, the latter had a lower ratio of contact points over surface grain area so a portion of the cementation is consumed on the surface of the grains, leading to a lower rate of reduction of permeability.

Although the sphericity of the particles is known to inhibit the flow (i.e., Kozeny–Carman equation), significant permeability differences were only observed in the case of angular sand in which the same reduction trend was observed with respect to the cementation level but shifted towards the higher permeability values. Fine and coarse glass beads behaved in a very similar manner to fine and very coarse subrounded sand showing that the dominating factor is the grain size in this case. The flow paths are affected by the grain shapes to some extent, however, the addition of cementation causes proportional reduction of permeability in either spheres, sub-rounded and angular sands.

5.4 Comparison of Properties of Artificial Specimens with Natural Sandstones

By varying the base materials, bio-treated specimens with various combinations of UCS, permeability and porosity are achieved covering a wide spectrum of properties as shown in Fig. 11, where UCS and permeability are plotted with respect to porosity. The porosity falls in the range between 0.2 and 0.45, while a UCS reaches a maximum value of approximately 4200 kPa. Permeability falls in the range between 10^{-2} and 10^{-8} m/s which coincides with the permeability range of soils to weakly cemented sands. Figure 11 presents also pairs of UCS and porosity, and of permeability and porosity values found in the literature. The widest trends identified in this study are also presented, bracketing the grey area and highlighting achievable strengths, permeabilities and porosities. A large portion of pairs reported in the literature fall in the region of achievable properties providing sufficient similarity with the average natural behaviour.

6 Conclusion

The selection of the base material in an MICP procedure contributes to delivering reliably artificially cemented soils of good quality and of various combinations of engineering properties which could be used as a proxy for natural weak sandstones or for designing field applications related to soil strengthening and controlled reduction of permeability based on the initial properties of the porous medium. This study investigated systematically the effects of the material's intrinsic properties on permeability, strength, and porosity of the bio-treated specimens utilising twelve base materials with various characteristics (grain size and shape, spread of the particle size distribution) across various cementation levels using a common MICP formulation to isolate the effects of those characteristics.

It is shown that better strength enhancement is achieved for bio-treated specimens with average grain sizes falling in the range between 180 and 890 μm registering values of UCS of about 500–2000 kPa across the cementation levels studied and final porosities from 0.28 to 0.38. Such grain sizes also allow for more control over permeability reduction providing more flow paths which are not very narrow. The optimum average grain size is 450 μm (moderate amount of contact points between particles), giving a UCS of about 2000 kPa

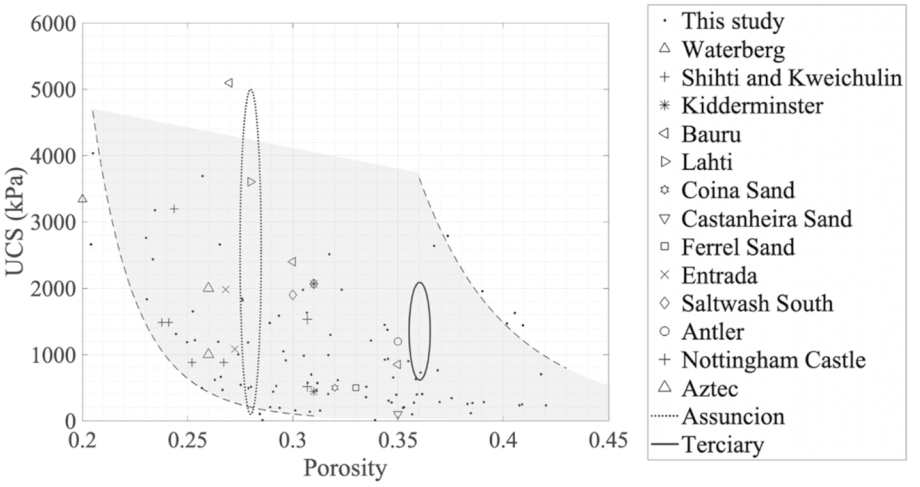

(a)

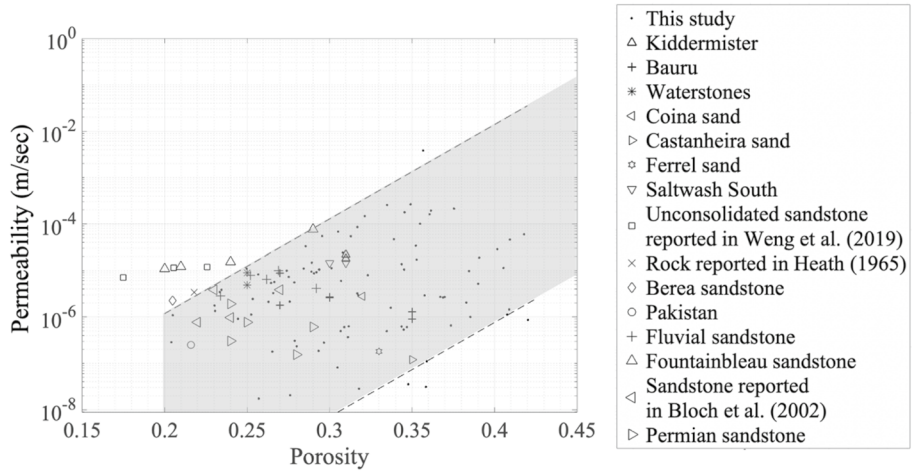

(b)

Fig. 11 **a** UCS and **b** permeability with respect to porosity. The diagrams include the findings of this study and values reported in the literature (Bloch et al. 2002; Bourbie and Zinszner 1985; Chen and Hu 2003; Dutton et al. 2003; Freitas and Dobereiner 1986; Heath 1965; Kanji 2014; Krishnan et al. 1998; Larsen 2015; Mohlala 2016; Pradhan et al. 2014; Prasad and Nur 2003; Raza et al. 2015; Sattler and Paraskevopoulou 2019; Suarez-Rivera et al. 2002; Weng et al. 2019)

and a permeability of 10^{-5} m/sec at 7.5% cementation while at 8.5% UCS is 2500 kPa and permeability is $8*10^{-5}$ m/sec.

Whilst more contact points provide a higher number of effective locations for cementation (e.g., very fine sands with an average particle size of 100 μm), too many contact points require more cementation to improve strength because any un-cemented contact points create a preferential path of failure during compression giving a lower strength. Very fine sands with an average particle size of 110 μm provide strength of

about 700 kPa at moderate cementation. Permeability decreases drastically when the cement is located on the contact points. For very fine sands, with more contact points across the particles, it is harder to reduce permeability since there are many contacts to be cemented, reducing permeability to about $5*10^{-7}$ m/sec (about only 5 times compared to the permeability of uncemented sand). Such materials provide self-regulation of flow through paths with larger pores and pore throats which are likely to un-cemented particle contacts.

Very coarse sands (D_{50} of 1810 μm) provide lower contact points between particles and hence a lower number of effective locations giving a lower strength (about 1000 kPa at 8% cementation) and show a less controlled reduction of permeability (10^{-5} m/sec at 8% cementation, a reduction that is sudden and starts at very low cementation levels).

The grain shape does not affect much the resulting strength permeability, though sub-rounded sands are optimum for strength gain and permeability control as fine spheres and fine sands show a very similar trend with values between 10^{-5} and 10^{-7} m/sec while the same behaviour is observed at larger grain sizes (similar trend and range of permeability between 10^{-6} and 10^{-4} m/sec). The UCS of glass beads is slightly lower than the one of corresponding rounded sands within the range of cementation levels investigated in this study.

Wider PSDs provide also better permeability control and strength enhancement as long as the number of contact points remains within the medium range. This can be achieved by mixing larger grain sizes at the aimed uniformity coefficient. Very high values of UCS up to 4000 kPa can be achieved with relatively high permeabilities ($5*10^{-4}$ to 10^{-6} m/sec) and porosities of about 0.25–0.33, provided that a larger amount of cementation exists. When the number of contact points remains large (i.e., mixture 1 with average particle size 371 μm) large permeability reduction is observed (values between 10^{-6} and 10^{-8} m/sec).

The MICP process is proven to be successful for materials that have been traditionally considered as inappropriate candidates for bio-cementation while various combinations of strengths, permeabilities and porosities were achieved. This study can potentially be useful to designing bio-treatment programs for controlled permeability reduction and strength enhancement in many hydraulic, hydrological, and geo-environmental engineering applications in shallow to moderate soil depths.

Acknowledgements This work has been carried out at the Department of Engineering at the University of Cambridge. The authors would like to acknowledge the funding and technical support from bp through the bp International Centre for Advanced Materials (bp-ICAM) which made this research possible. Y.W. acknowledges the financial support of Natural Science Foundation of China (Grant Nos. 52171262, 42141003) and Science and Technology Innovation Committee of Shenzhen (Grant No. JCYJ20210324103812033) and Southern Marine Science and Engineering Guangdong Laboratory (Guangzhou, Grant No. K19313901) for conducting this study.

Authors Contributions CK contributed to conceptualization, methodology, data curation, software, formal analysis, writing—original draft, writing—review and editing, and visualization. YW contributed to conceptualization, methodology, writing—review and editing, and funding acquisition. GB contributed to conceptualization, supervision, funding acquisition, writing—reviewing and editing.

Declarations

Conflict of interest The authors declare that they have no known competing financial interests or personal relationships that could have appeared to influence the work reported in this paper.

References

Al Qabany, A., Soga, K.: Effect of chemical treatment used in MICP on engineering properties of cemented soils. Geotechnique **63**, 331–339 (2013). https://doi.org/10.1680/geot.SIP13.P.022

Al Qabany, A., Soga, K., Santamarina, C.: Factors affecting efficiency of microbially induced calcite precipitation. J. Geotech. Geoenviron. Eng. **138**, 992–1001 (2012). https://doi.org/10.1061/(ASCE)GT.1943-5606.0000666

Alqahtani, N.J., Niu, Y., da Wang, Y., Chung, T., Lanetc, Z., Zhuravljov, A., Armstrong, R.T., Mostaghimi, P.: Super-resolved segmentation of X-ray images of carbonate rocks using deep learning. Transp. Porous Media (2022). https://doi.org/10.1007/s11242-022-01781-9

ASTM: Compressive strength and elastic moduli of intact rock core specimens under varying states of stress and temperatures. Stress Int. J. Biol. Stress (2004). https://doi.org/10.1520/D7012-14.1.5.1.1

ASTM: Standard test method for rapid determination of carbonate content of soils. ASTM Int. (2014). https://doi.org/10.1520/D4373-14

Barkouki, T.H., Martinez, B.C., Mortensen, B.M., Weathers, T.S., de Jong, J.D., Ginn, T.R., Spycher, N.F., Smith, R.W., Fujita, Y.: Forward and inverse bio-geochemical modeling of microbially induced calcite precipitation in half-meter column experiments. Transp. Porous Media **90**, 23–39 (2011). https://doi.org/10.1007/s11242-011-9804-z

Bloch, S., Lander, R.H., Bonnell, L.: Anomalously high porosity and permeability in deeply buried sandstone reservoirs: origin and predictability (2002)

Bourbie, T., Zinszner, B.: Hydraulic and acoustic properties as a function of porosity in Fontainebleau Sandstone. J. Geophys. Res. **90**, 11524 (1985). https://doi.org/10.1029/jb090ib13p11524

Burbank, M., Kavazanjian, E., Weaver, T., Montoya, B.M., Hamdan, N., Bang, S.S., Esnault-Filet, A., Tsesarsky, M., Aydilek, A., Ciurli, S., Tanyu, B., Manning, D.A.C., Larrahondo, J., Soga, K., Chu, J., Dejong, J.T., Cheng, X., Kuo, M., AlQabany, A., Seagren, E.A., Van Paassen, L.A., Renforth, P., Laloui, L., Nelson, D.C., Hata, T., Burns, S., Chen, C.Y., Caslake, L.F., Fauriel, S., Jefferis, S., Santamarina, J.C., Inagaki, Y., Martinez, B., Palomino, A.: Biogeochemical processes and geotechnical applications: progress, opportunities and challenges. Géotechnique **63**, 287–301 (2013). https://doi.org/10.1680/geot.SIP13.P.017

Chen, H., Hu, Z.Y.: Some factors affecting the uniaxial strength of weak sandstones. Bull. Eng. Geol. Environ. **62**, 323–332 (2003). https://doi.org/10.1007/s10064-003-0207-4

Cheng, L., Cord-Ruwisch, R., Shahin, M.A.: Cementation of sand soil by microbially induced calcite precipitation at various degrees of saturation. Can. Geotech. J. **50**, 81–90 (2013). https://doi.org/10.1139/cgj-2012-0023

Cheng, L., Shahin, M.A., Mujah, D.: Influence of key environmental conditions on microbially induced cementation for soil stabilization. J. Geotech. Geoenviron. Eng. **143**, 04016083 (2017). https://doi.org/10.1061/(ASCE)GT.1943-5606.0001586

Cui, M.J., Zheng, J.J., Zhang, R.J., Lai, H.J., Zhang, J.: Influence of cementation level on the strength behaviour of bio-cemented sand. Acta Geotech. **12**, 971–986 (2017). https://doi.org/10.1007/s11440-017-0574-9

Dadda, A., Geindreau, C., Emeriault, F., Rollanddu Roscoat, S., Esnault Filet, A., Garandet, A.: Characterization of contact properties in biocemented sand using 3D X-ray micro-tomography. Acta Geotech. **14**, 597–613 (2019). https://doi.org/10.1007/s11440-018-0744-4

de Freitas, M.H., Dobereiner, L.: Geotechnical properties of weak sandstones. Géotechnique **36**, 79–94 (1986). https://doi.org/10.1680/geot.1986.36.1.79

DeJong, J.T., Mortensen, B.M., Martinez, B.C., Nelson, D.C.: Bio-mediated soil improvement. Ecol Eng. **36**, 197–210 (2010). https://doi.org/10.1016/j.ecoleng.2008.12.029

Doube, M., Klosowski, M.M., Arganda-Carreras, I., Cordelières, F.P., Dougherty, R.P., Jackson, J.S., Schmid, B., Hutchinson, J.R., Shefelbine, S.J.: BoneJ: free and extensible bone image analysis in ImageJ. Bone (2010). https://doi.org/10.1016/j.bone.2010.08.023

Dougherty, R., Kunzelmann, K.-H.: Computing local thickness of 3D structures with ImageJ. Microsc. Microanal. **13**, 1678–1679 (2007). https://doi.org/10.1017/s1431927607074430

Dutton, S.P., Flanders, W.A., Barton, M.D.: Reservoir characterization of a Permian deep-water sandstone, East Ford field, Delaware Basin, Texas. Am. Assoc. Petrol. Geol. Bull. **87**, 609–627 (2003). https://doi.org/10.1306/10100201085

Feng, K., Montoya, B.M.: Influence of confinement and cementation level on the behavior of microbial-induced calcite precipitated Sands under monotonic drained loading. J. Geotech. Geoenviron. Eng. **142**, 04015057 (2015). https://doi.org/10.1061/(ASCE)GT.1943-5606.0001379

Gao, Y., Hang, L., He, J., Chu, J.: Mechanical behaviour of biocemented sands at various treatment levels and relative densities. Acta Geotech. **14**, 697–707 (2019). https://doi.org/10.1007/s11440-018-0729-3

Gao, Y., Raeini, A.Q., Selem, A.M., Bondino, I., Blunt, M.J., Bijeljic, B.: Pore-scale imaging with measurement of relative permeability and capillary pressure on the same reservoir sandstone sample under water-wet and mixed-wet conditions. Adv. Water Resour. **146**, 15 (2020). https://doi.org/10.1016/j.advwatres.2020.103786

Heath, L.J.: Variations in permeability and porosity of synthetic oil reservoir rock—methods of control. Soc. Petrol. Eng. J. **5**, 329–332 (1965)

Hussain, F., Pinczewski, W.V., Cinar, Y., Arns, J.Y., Arns, C.H., Turner, M.L.: Computation of relative permeability from imaged fluid distributions at the pore scale. Transp. Porous Media **104**, 91–107 (2014). https://doi.org/10.1007/s11242-014-0322-7

Ismail, M.A., Joer, H.A., Randolph, M.F., Meritt, A.: Cementation of porous materials using calcite. Géotechnique. **52**, 313–324 (2002). https://doi.org/10.1680/geot.2002.52.5.313

ISRM: Basic geotechnical description of rock masses. Int. J. Rock Mech. Min. Sci. **25**, 85–110 (1981)

Kanji, M.A.: Engineering works affected by soft rocks. In: ISRM Conference on Rock Mechanics for Natural Resources and Infrastructure, SBMR 2014. Goiania, Brazil (2014)

Konstantinou, C., Biscontin, G.: Experimental investigation of the effects of porosity, hydraulic conductivity, strength, and flow rate on fluid flow in weakly. Hydrology **9**(11), 190 (2022). https://doi.org/10.3390/hydrology9110190

Konstantinou, C., Biscontin, G., Jiang, N.-J., Soga, K.: Application of microbially induced carbonate precipitation (MICP) to form bio-cemented artificial sandstone. J. Rock Mech. Geotech. Eng. (2021a). https://doi.org/10.1016/j.jrmge.2021.01.010

Konstantinou, C., Biscontin, G., Logothetis, F.: Tensile strength of artificially cemented sandstone generated via microbially induced carbonate precipitation. Materials **14**, 4735 (2021b). https://doi.org/10.3390/ma14164735

Konstantinou, C., Wang, Y., Biscontin, G., Soga, K.: The role of bacterial urease activity on the uniformity of carbonate precipitation profiles of bio-treated coarse sand specimens. Sci. Rep. **11**, 1–17 (2021c). https://doi.org/10.1038/s41598-021-85712-6

Konstantinou, C., Biscontin, G.: Soil enhancement via microbially induced calcite precipitation. In: Proceedings of the 10th International Symposium on Geotechnical Aspects of Underground Construction in Soft Ground, pp. 765–772. Taylor & Francis, Cambridge (2021)

Konstantinou, C.: Hydraulic fracturing of artificially generated soft sandstones, Ph.D. thesis, University of Cambridge (2020). https://doi.org/10.17863/CAM.64233

Krishnan, G.R., Zhao, X.L., Zaman, M., Roegiers, J.C.: Fracture toughness of a soft sandstone. Int. J. Rock Mech. Min. Sci. **35**, 695–710 (1998). https://doi.org/10.1016/S0148-9062(97)00324-0

Larsen, E.B.: Geomechanical and Structural characteristics of a paleoreservoir-caprock sucsession (2015)

Lima, M.C.O., Pontedeiro, E.M., Ramirez, M., Boyd, A., van Genuchten, M.T., Borghi, L., Couto, P., Raoof, A.: Petrophysical correlations for the permeability of coquinas (carbonate rocks). Transp. Porous Media **135**, 287–308 (2020). https://doi.org/10.1007/s11242-020-01474-1

Liu, Q., Hu, R., Hu, L., Xing, Y., Qiu, P., Yang, H., Fischer, S., Ptak, T.: Investigation of hydraulic properties in fractured aquifers using cross-well travel-time based thermal tracer tomography: numerical and field experiments. J. Hydrol. (amst.) **609**, 10 (2022). https://doi.org/10.1016/j.jhydrol.2022.127751

Mahawish, A., Bouazza, A., Gates, W.P.: Effect of particle size distribution on the bio-cementation of coarse aggregates. Acta Geotech. **13**, 1019–1025 (2018a). https://doi.org/10.1007/s11440-017-0604-7

Mahawish, A., Bouazza, A., Gates, W.P.: Improvement of coarse sand engineering properties by microbially induced calcite precipitation. Geomicrobiol. J. **35**, 887–897 (2018b). https://doi.org/10.1080/01490451.2018.1488019

Marzin, T., Desvages, B., Creppy, A., Lépine, L., Esnault-Filet, A., Auradou, H.: Using microfluidic setup to determine the adsorption rate of *Sporosarcina pasteurii* bacteria on sandstone. Transp. Porous Media **132**, 283–297 (2020). https://doi.org/10.1007/s11242-020-01391-3

Mitchell, J.K., Santamarina, J.C.: Biological considerations in geotechnical engineering. J. Geotech. Geoenviron. Eng. **131**, 1222–1233 (2005). https://doi.org/10.1061/(ASCE)1090-0241(2005)131:10(1222)

Mohlala, K.: Effects of Porosity on Strength of Sandstones. Hammanskraal and Waterberg (2016)

Mortensen, B.M., Haber, M.J., Dejong, J.T., Caslake, L.F., Nelson, D.C.: Effects of environmental factors on microbial induced calcium carbonate precipitation. J. Appl. Microbiol. **111**, 338–349 (2011). https://doi.org/10.1111/j.1365-2672.2011.05065.x

Mujah, D., Shahin, M.A., Cheng, L.: State-of-the-art review of biocementation by microbially induced calcite precipitation (MICP) for soil stabilization. Geomicrobiol. J. **34**, 524–537 (2017). https://doi.org/10.1080/01490451.2016.1225866

van Paassen, L.: Biogrout: Ground Improvement by Microbially Induced Carbonate Precipitation. Ph.D. thesis, Delft University of Technology (2009)

Pradhan, S., Stroisz, A.M., Fjær, E., Stenebraten, J., Lund, H.K., Sønstebø, E.F., Roy, S.: Fracturing tests on reservoir rocks: analysis of AE events and radial strain evolution. In: 48th US Rock Mechanics/Geomechanics Symposium 2014, pp. 45–49, Minneapolis (2014)

Prasad, M., Nur, A.: Velocity and attenuation anisotropy in reservoir rocks: 73rd annual (2003)

Raza, A., Bing, C.H., Nagarajan, R., Hamid, M.A.: Experimental investigation on sandstone rock permeability of Pakistan gas fields. In: IOP Conference Series: Materials Science and Engineering. Institute of Physics Publishing (2015)

Rebata-Landa, V.: Microbial Activity in Sediments: Effects on Soil Behavior (2007)

Rubol, S., Tonina, D., Vincent, L., Sohm, J.A., Basham, W., Budwig, R., Savalia, P., Kanso, E., Capone, D.G., Nealson, K.H.: Seeing through porous media: an experimental study for unveiling interstitial flows. Hydrol. Process. **32**, 402–407 (2018). https://doi.org/10.1002/hyp.11425

Rueden, C.T., Schindelin, J., Hiner, M.C., DeZonia, B.E., Walter, A.E., Arena, E.T., Eliceiri, K.W.: Image J2: ImageJ for the next generation of scientific image data. BMC Bioinform. **18**, 1–26 (2017). https://doi.org/10.1186/s12859-017-1934-z

Sattler, T., Paraskevopoulou, C.: Implications on characterizing the extremely weak sherwood sandstone: case of slope stability analysis using SRF at two oak quarry in the UK. Geotech. Geol. Eng. **37**, 1897–1918 (2019). https://doi.org/10.1007/s10706-018-0732-3

Saxena, N., Hows, A., Hofmann, R., Alpak, F.O., Dietderich, J., Appel, M., Freeman, J., de Jong, H.: Rock properties from micro-CT images: Digital rock transforms for resolution, pore volume, and field of view. Adv. Water Resour. (2019a). https://doi.org/10.1016/j.advwatres.2019.103419

Saxena, N., Hows, A., Hofmann, R., Freeman, J., Appel, M.: Estimating pore volume of rocks from pore-scale imaging. Transp. Porous Media **129**, 403–412 (2019b). https://doi.org/10.1007/s11242-019-01295-x

Schindelin, J., Arganda-Carreras, I., Frise, E., Kaynig, V., Longair, M., Pietzsch, T., Preibisch, S., Rueden, C., Saalfeld, S., Schmid, B., Tinevez, J.Y., White, D.J., Hartenstein, V., Eliceiri, K., Tomancak, P., Cardona, A.: Fiji: an open-source platform for biological-image analysis. Nat. Methods **9**, 676–682 (2012). https://doi.org/10.1038/nmeth.2019

Scott, G., Wu, K., Zhou, Y.: Multi-scale image-based pore space characterisation and pore network generation: case study of a North Sea sandstone reservoir. Transp. Porous Media **129**, 855–884 (2019). https://doi.org/10.1007/s11242-019-01309-8

Suarez-Rivera, R., Stenebråten, J., Gadde, P.B., Sharma, M.M.: An Experimental investigation of fracture propagation during water injection. In: International Symposium and Exhibition on Formation Damage Control, pp. 1–11. Lafayette, Louisiana (2002)

Terzis, D., Laloui, L.: 3-D micro-architecture and mechanical response of soil cemented via microbial-induced calcite precipitation. Sci. Rep. **8**, 1–11 (2018). https://doi.org/10.1038/s41598-018-19895-w

Terzis, D., Laloui, L.: Cell-free soil bio-cementation with strength, dilatancy and fabric characterization. Acta Geotech. **14**, 639–656 (2019). https://doi.org/10.1007/s11440-019-00764-3

Tobler, D.J., Minto, J.M., el Mountassir, G., Lunn, R.J., Phoenix, V.R.: Microscale analysis of fractured rock sealed with microbially induced $CaCO_3$ precipitation: influence on hydraulic and mechanical performance. Water Resour. Res. **54**, 8295–8308 (2018). https://doi.org/10.1029/2018WR023032

Torskaya, T., Shabro, V., Torres-Verdín, C., Salazar-Tio, R., Revil, A.: Grain shape effects on permeability, formation factor, and capillary pressure from pore-scale modeling. Transp. Porous Media **102**, 71–90 (2014). https://doi.org/10.1007/s11242-013-0262-7

van Wijngaarden, W.K., van Paassen, L.A., Vermolen, F.J., van Meurs, G.A.M., Vuik, C.: A reactive transport model for Biogrout compared to experimental data. Transp. Porous Media **111**, 627–648 (2016). https://doi.org/10.1007/s11242-015-0615-5

Wang, M., Kulatilake, P.H.S.W.: Understanding of hydraulic properties from configurations of stochastically distributed fracture networks. Hydrol. Process. **22**, 1125–1135 (2008). https://doi.org/10.1002/hyp.6667

Wang, X., Nackenhorst, U.: A coupled bio-chemo-hydraulic model to predict porosity and permeability reduction during microbially induced calcite precipitation. Adv. Water Resour. (2020). https://doi.org/10.1016/j.advwatres.2020.103563

Wang, Y., Soga, K., Dejong, J.T., Kabla, A.J.: Micro-scale visualization of microbial-induced calcium carbonate precipitation processes. J. Geotech. Geoenviron. Eng. **145**, 04019045 (2019). https://doi.org/10.1061/(ASCE)GT.1943-5606.0002079

Wang, Y., Soga, K., Dejong, J.T., Kabla, A.J.: Effects of bacterial density on growth rate and characteristics of microbial-induced $CaCO_3$ precipitates: a particle-scale experimental study. ASCE J. Geotech. Geoenviron. Eng. **14**, 7 (2021). https://doi.org/10.1016/(ASCE)GT.1943-5606.0002509

Wang, C., Wu, K., Scott, G.G., Jia, A.: Merge pore clusters: a novel method to construct pore networks and predict permeability from 2D rock images. Adv. Water. Resour. **166**, 104238 (2022a). https://doi.org/10.1016/j.advwatres.2022.104238

Wang, Y., Konstantinou, C., Soga, K., Biscontin, G., Kabla, A.J.: Use of microfluidic experiments to optimize MICP treatment protocols for effective strength enhancement of MICP-treated sandy soils. Acta Geotech. **17**, 3817–3838 (2022b). https://doi.org/10.1007/s11440-022-01478-9

Weinhardt, F., Class, H., Vahid Dastjerdi, S., Karadimitriou, N., Lee, D., Steeb, H.: Experimental methods and imaging for enzymatically induced calcite precipitation in a microfluidic cell. Water Resour. Res. **5**, 7 (2021). https://doi.org/10.1029/2020WR029361

Weng, H.Y., Deng, J.G., Tan, Q., Liu, H.L.: Deformation characteristics of unconsolidated sandstone and soft mudstone and their effects on drilling engineering. In: 53rd U.S. Rock Mechanics/Geomechanics Symposium. pp. 1–7, New York (2019)

Xiao, Y., Asce, M., Stuedlein, A.W., Asce, M., Ran, J., Evans, T.M., Asce, A.M., Cheng, L., Liu, H., Paassen, L.A.V., Chu, J., Asce, M.: Effect of particle shape on strength and stiffness of biocemented glass beads. J. Geotech. Geoenviron. Eng. **145**, 1–9 (2019). https://doi.org/10.1061/(ASCE)GT.1943-5606.0002165

Yu, C., Tran, H., Sakhaee-Pour, A.: Pore size of shale based on acyclic pore model. Transp. Porous Media **124**, 345–368 (2018). https://doi.org/10.1007/s11242-018-1068-4

Zhao, H., Luo, N., Illman, W.A.: The importance of fracture geometry and matrix data on transient hydraulic tomography in fractured rocks: Analyses of synthetic and laboratory rock block experiments. J. Hydrol. (amst.) (2021). https://doi.org/10.1016/j.jhydrol.2021.126700

Authors and Affiliations

Charalampos Konstantinou[1,2] · Yuze Wang[3,4] · Giovanna Biscontin[1]

✉ Charalampos Konstantinou
ckonst06@ucy.ac.cy; charalambosconst@gmail.com

✉ Yuze Wang
wangyz@sustech.edu.cn

Giovanna Biscontin
gb479@cam.ac.uk

[1] Department of Engineering, University of Cambridge, Cambridge, UK

[2] Present Address: Department of Civil and Environmental Engineering, University of Cyprus, Nicosia, Cyprus

[3] Department of Ocean Science and Engineering, Southern University of Science and Technology, Shenzhen, China

[4] Southern Marine Science and Engineering Guangdong Laboratory (Guangzhou), Guangzhou, China